Experimental Investigation of Isolated Roughness Induced Transition in a Swept Wing Boundary Layer

Zoppini, G.; Ragni, D.; Kotsonis, M.

DOI
10.2514/6.2022-1213

Publication date
2022

Document Version
Final published version

Published in
AIAA SCITECH 2022 Forum

Citation (APA)
Zoppini, G., Ragni, D., & Kotsonis, M. (2022). Experimental Investigation of Isolated Roughness Induced Transition in a Swept Wing Boundary Layer. In *AIAA SCITECH 2022 Forum* Article AIAA 2022-1213 (AIAA Science and Technology Forum and Exposition, AIAA SciTech Forum 2022). https://doi.org/10.2514/6.2022-1213

AIAA SciTech Forum
January 3-7, 2022, San Diego, CA & Virtual
AIAA SCITECH 2022 Forum

10.2514/6.2022-1213

Experimental Investigation of Isolated Roughness Induced Transition in a Swept Wing Boundary Layer

G. Zoppini *, D. Ragni † and M. Kotsonis ‡
Delft University of Technology, Delft, The Netherlands, 2629HS

The application of an isolated roughness element in the laminar boundary layer developing on the surface of a wing, introduces flow instabilities that eventually lead to the breakdown of the laminar flow structures and the formation of a turbulent wedge. The present work, investigates the instabilities and transition process initiated by an isolated roughness element applied in a swept wing boundary layer. Specifically, the perturbations induced by a cylindrical element are analysed, providing relevant insights regarding the nature of the instabilities developing in the flow field. The global flow features are measured through infrared thermography, while local information on the stationary and unsteady disturbances are provided by hot wire anemometry. The collected results, prove that the main instabilities responsible for the wedge origin and evolution are related to the shedding process initiated in the wake of the roughness element. Additionally, the dominant flow features identified in the present work, show significant similarities with those pertaining to 2D boundary layer transition initiated by isolated roughness elements.

Nomenclature

α = Angle of attack, deg.
c_X = Streamwise chord, m.
δ^* = Boundary-layer displacement thickness, mm.
Re_k = Roughness Reynolds number, $\frac{|\mathbf{u}(k)|k}{\nu}$.
$\overline{U}_\infty$ = Free-stream velocity, ms^{-1}.
X, Y, Z = Reference coordinate system parallel to the wind tunnel floor.
x, y, z = Reference coordinate system orthogonal to the leading edge.

c = Leading edge orthogonal chord, m.
D = Element diameter, mm.
k = Element height, mm.
Re_{c_X} = Reynolds number, $\frac{\overline{U}_\infty c_X}{\nu}$.
St_k = Roughness Strouhal number, $\frac{f\,k}{|\mathbf{u}(k)|}$.

I. Introduction

Surface roughness is a parameter that plays a fundamental role in the laminar-to-turbulent transition process of two- or three-dimensional boundary layers (BL). Specifically, previous investigations [1–5] observed that a sufficiently large isolated roughness element applied on the surface of a wing, leads to transition via the formation and spreading of a turbulent wedge. Numerous works [e.g. 4, 6] focussed on determining *a priori* the influence of the roughness element geometry on the flow, eventually defining the roughness Reynolds number Re_k as a predicting parameter.

Detailed experimental and numerical investigations have been dedicated to the characterization of the flow topology induced by an isolated roughness element in 2D boundary layers [1–4, 7]. The conducted studies, showed that the presence of the roughness element in an otherwise laminar boundary layer initiates a momentum redistribution process. In particular, the spanwise vorticity pertaining to the undisturbed BL rolls up upstream of the element, forming a horseshoe vortex system (HSV) with two steady counter-rotating legs extending downstream. The two HSV legs promote the momentum redistribution process based on the the lift-up mechanism [8], causing the upwards deflection of low speed flow. The downstream development of these structures results in a flow configuration dominated by the alternation of low- and high-speed streaks, which destabilize the edges of the turbulent flow region, enhancing its spanwise spreading [e.g. 5, 9]. The spectral analysis of the collected hot wire data identifies an oscillatory behaviour of

---

[*] PhD Candidate, Section of Aerodynamics, Faculty of Aerospace Engineering, AIAA Student Member.
[†] Asossciate Professor, Section of Aeroacoustics, Faculty of Aerospace Engineering
[‡] Asossciate Professor, Section of Aerodynamics, Faculty of Aerospace Engineering

the horseshoe legs [3], dominated by frequency peaks that correspond to those of the roughness cylinder shedding. Further investigations [4, 10] proved that a process of hairpin vortex shedding is initiated by the separated flow region located on top of the element. Periodic shedding is observed for a wide range of Strouhal numbers (St=0.1-0.4, computed based on the shedding frequency, the elements height or radius and the local boundary layer velocity extracted on top of the element), with appearance of harmonics of the dominant modes and of secondary instabilities, all growing in amplitude with Re_k. These results were confirmed and extended by recent DNS [7, 9] and experiments [5, 11–13].

The body of work dedicated to to isolated roughness elements located in a swept wing boundary layer [e.g. 14–16], is less extensive than the literature available on 2D boundary layers transition. Most of the available works, analyse the mechanisms leading to the wedge formation [17] and development, focussing on the low-/high- speed streaks cascade occurring at the wedge edges [5]. By investigating the flow topology aft of the roughness element, a single streak developing downstream of the element is identified in the flow field. Interestingly, the downstream evolution of this streak occurs with direction and behavior comparable to those typical of crossflow vortices. The DNS by [18] reaches similar conclusions, additionally identifying the high shear region located on top of the element to be responsible for initiating the instabilities leading to the laminar breakdown. This suggests that strong similarities of the near-element flow features characterize isolated elements in 2D and 3D boundary layers [19]. However, the downstream development of the flow field is characterized by a strong asymmetry, as observed in DNS flow investigations conducted both by [18] and [19]. In particular, the crossflow direction of rotation appears to be favoured in 3D boundary layers, leading to the development of a flow field dominated by structures co-rotating with the crossflow. This introduces significant differences between 2D and 3D boundary layers when considering the downstream flow evolution.

The present work experimentally investigates the transition scenario induced by a cylindrical isolated roughness element located in a swept wing boundary layer. The near-element flow field is measured in order to identify the dominant flow features and characterize the nature of the developing instabilities. Measurements are performed for three different Re_k numbers, allowing for investigating the flow behavior in a super-critical forcing configuration (i.e. a roughness configuration causing flow tripping shortly after the element location) and a critical forcing configuration (i.e. a roughness configuration introducing instabilities that grow and eventually lead to laminar breakdown). The characterization of the base flow topology is performed though infrared thermography, providing information regarding the turbulent wedge onset location and chordwise development. Additionally, to detail the dominant flow features ensuing in the near-element wake, including the developing stationary and unsteady instabilities, local hot wire anemometry measurements are performed. Specifically, the acquired time-dependent velocity signal allows for spectral analysis of the velocity fluctuations, fundamental towards the understanding of the nature and evolution of the developing instabilities.

II. Methodology

A. Wing Model and Wind Tunnel Facility

The present work is based on experimental measurements conducted in the low speed Low Turbulence wind Tunnel (LTT) located at the TU Delft, an atmospheric closed return tunnel featuring a low freestream turbulence level in the test section flow [20]. The measured wind tunnel model is a constant-chord swept wing (M3J) extensively described by [20]. The wing is purposely designed to develop a 3D boundary layer whose transitional process is dominated by crossflow type of instabilities. The acquisitions are performed for a chosen angle of attack (α=-3.36°) and variable freestream Reynolds numbers: $\mathrm{Re}_{c_X}=1.27\times10^6$, 1.35×10^6, 1.45×10^6. A numerical steady and incompressible boundary layer solution is also computed at each Re_{c_X} measured, following an in-house developed procedure fully described in [21].

Two different coordinate reference systems are defined for this wing model: one has its z-axis aligned to the leading edge with spatial components xyz and velocity u, v, w; the second one is integral with the wind tunnel floor, with spatial components given by XYZ and velocity components U, V, W.

B. Isolated Roughness Element

The geometrical parameters of the isolated roughness element employed in the present study, are defined based on previous experimental investigations [i.e. 16, 22]. A single cylindrical element with diameter D≃6mm and height k≃0.5mm is applied on the wing surface at a chordwise station x/c=0.15 (with c=1273mm being the streamwise wing chord). The roughness element was produced by machining copper rods with the same diameter D [22].

A well established parameter describing the element geometry with respect to the BL evolution, is the roughness Reynolds number [1, 4, 6]. This parameter offers a purely geometrical scaling, and is defined as $\mathrm{Re}_k = \frac{k\times|\mathbf{u}(k)|}{\nu}$ with

$|\mathbf{u}(k)|$ boundary layer velocity at the element height and ν kinematic viscosity. In particular, the Re_k value referring to a particular forcing configuration can be related with its critical value, namely the lower Re_k value describing a roughness geometry causing boundary layer flow tripping to turbulence. From previous literature studies, the critical Re_k is found to scale with $(\mathrm{k/D})^{2/5}$, starting from values of $\mathrm{Re}_{k,crit}$ = 600-900 for an element with k/D=1 [e.g. 4, 13]. Based on the element k/D ratio of the present set-up (kept constant at ≃0.08), the corresponding $\mathrm{Re}_{k,crit}$ range lays between 225 and 335. Therefore, the three different Re_{cx} measured in the present investigation, correspond to Re_{k_1}=251 (super-critical), Re_{k_2}=219 and Re_{k_3}=198 (critical).

C. Measurement Techniques and Data Analysis

1. Infra-red Thermography

Infrared thermography [e.g. 14, 16] is employed in the present investigation to image the wing surface temperature, and its modifications due to external heat deposition. This method is based on the Reynold's analogy, relating the warmer (colder) regions of the wing surface to laminar (turbulent) flow regions, as they are characterized by a lower (higher) convective heat transfer coefficient. The acquired images provide a global overview of the developing flow features, indicating whether turbulent transition occurs in the flow.

The measurements are performed with an Optris PI640 IR camera, imaging the pressure side of the model through an opening in the test section side wall. The camera is equipped with a wide angle lens, f=10.5 mm, which captures a field of view centred at the wing midspan and extending from the leading edge to the trailing edge of the wing. The resulting resolution is 0.85mm/px. For each of the considered Re_k, 80 images are acquired with a frequency of 4Hz. During the acquisition, five external halogen lamps (3 × 400W and 2 × 500W) are used to actively heat the model surface in order to improve the thermal contrast between the laminar and turbulent BL region. The images collected for the three different Re_k are then averaged to reduce the signal to noise ratio, and are geometrically mapped to the *XYZ* Cartesian framework by applying an in-house calibration procedure.

2. Hot Wire Anemometry

To fully characterize the developing steady and unsteady perturbations, hot-wire anemometry (HWA) measurements are performed using a single-wire boundary layer probe (Dantec Dynamics 55P15). The sensor is operated using a TSI IFA-300 constant temperature bridge with automatic adjustment of the overheat ratio. The wire is mounted on an automated traverse system installed in the wind tunnel diffuser having three degrees-of-freedom with a step resolution of 2.5μm.

The HWA velocity fields are acquired at various chord locations in the zy plane. Each constant chord plane consists of an ensemble of hot-wire scans of the developing boundary layer acquired for a fixed span-wise location in the wall-normal direction. Each BL profile is composed of 30 point-wise measurements spanning from the wall vicinity to the inviscid flow, acquired at equally-spaced y-locations. The velocity signal is sampled for 2s at a frequency of 51.2kHz, and is low passed filtered with a cutoff frequency of 20kHz before being amplified. As moving towards downstream x/c locations, the y-spacing between successive measurement points is adjusted to account for the BL growth, thus covering the boundary layer extent from the near-wall region (≃ 20% U_∞) to the local freestream. The final spacing changes from 0.1mm for the near element planes (x/c=0.158, 0.162, 0.166, 0.170) to 0.15mm for the more downstream planes (x/c=0.18, 0.19, 0.20, 0.25). After completing the acquisition of a full BL profile, the probe is moved to the next spanwise location, repeating the measurement procedure to acquire the set number of boundary layer scans. Specifically, the analysis of the infra-red images provides an estimation of the developing wedge expansion and orientation, allowing for adjustment of the origin and span-wise extent of the measured zy domain at each chord location. Accordingly, the spanwise spatial resolution results in 0.5mm for the near-element planes corresponding to a total spanwise extent of 30mm, while it is set to 1mm for the more downstream acquisitions.

Throughout this study, the hot-wire probe is aligned to the Z direction. Hence, the point-wise measured velocity signal is a projection of the instantaneous velocity components that can be reconstructed as equation 1.

$$\overline{U}(y,z) = \sqrt{(u \times cos(45°) + (w \times sin(45°))^2 + (v)^2} \tag{1}$$

The acquired HWA signal is then time-averaged to investigate the stationary velocity fields ($\overline{U}(z,y)$), and is normalized by the time-averaged freestream velocity extracted at the corresponding x/c ($\overline{U}_\infty$). The non-dimensional y and z are instead defined as $\mathrm{y}/\overline{\delta}^*$ and $\mathrm{z}/\overline{\delta}^*$ with $\overline{\delta}^*$=0.593mm being the displacement thickness of the experimentally measured

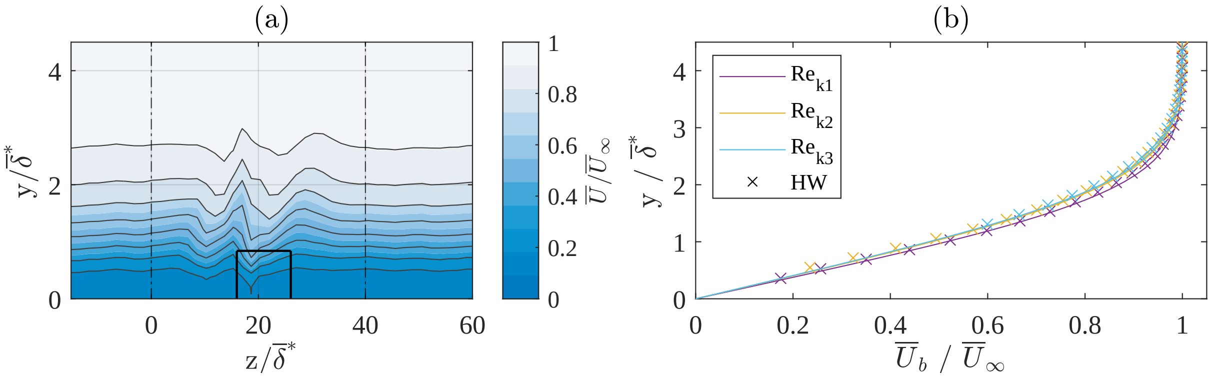

Fig. 1 (a) Time-averaged HWA velocity contours for Re$_{k_2}$ at x/c=0.2. Velocity isolines every 10% of $\overline{U}_\infty$ (gray lines); sketch of the element location (black rectangle); limits of the perturbed flow region (vertical -. lines). (b) Comparison of HWA (×) and numerical (-) boundary layer velocity profile at x/c=0.2.

laminar boundary layer at x/c=0.158 and Re$_{k_1}$. At each chord location, the acquired velocity field extends in the spanwise direction on both sides of the perturbed flow region, thus including a portion of the undisturbed laminar boundary layer (figure 1(a)). Hence, the boundary layer development ($\overline{U}_b(y)$) is estimated at each chord location as the spanwise average of the velocity signal in the unperturbed flow region. Moreover, assuming a linear trend in the near-wall region, the resulting BL velocity profile is linearly extrapolated to find the y-value where $\overline{U}_b(y)$=0, which is identified as the wall location. Additionally, the steady boundary layer disturbance field is defined as $\overline{U}_d(y,z) = \overline{U}(y,z)$- $\overline{U}_b(y)$, allowing for further processing of the data to isolate the high-speed and low-speed regions of the flow, tracking their downstream evolution.

The analysis of the time dependent velocity signal provides information regarding the unsteady disturbances evolution. Specifically, the velocity fluctuation fields (U') identify the regions of highest fluctuation. By extracting the corresponding frequency spectra, information regarding the dominant fluctuations frequencies along with their harmonics can be retrieved. The results of the described data analysis are discussed in § IV.

III. Flow Field Topology

A. Base Flow Evolution

The assessment of the base flow (i.e. unperturbed boundary layer) in the present work, is performed both experimentally and numerically by computing a numerical boundary layer solution for each of the three measured Re$_k$. The numerical BL is computed by solving the steady and incompressible spanwise-invariant boundary layer equations, based on the experimentally acquired free-stream flow characteristics and measured pressure distribution [21]. The laminar boundary layer velocity profile $\overline{U}_b$ extracted from the time-averaged HWA data, is compared with the numerical BL velocity transformed to the hot-wire measurement system following equation 1 in figure 1(b).

The infrared thermography data, allow for further characterization of the base flow, providing preliminary information regarding the turbulent flow region origin and evolution (figure 2). For the three considered Re$_k$, the IR images show the roughness element as a low-temperature dot located at x/c=0.15. Aft of the element, the flow field develops into a turbulent region, which is deflected towards the wing root as evolving downstream. This introduces asymmetric flow features which differ from the typical development of the 2D boundary layer scenario [3, 19]. The developing turbulent flow region eventually evolves into a turbulent wedge, which appears in the thermographic images as a region of low temperature. Hence, to quantify the wedge development and determine its width and opening angle, individual temperature profiles are extracted from the IR fields along z-parallel lines and compared to a predefined threshold. To perform this analysis a set of chord locations is chosen between x/c=0.158-0.35, and the resulting estimations are reported as symbols superimposed to the IR images of figure 2. The wedge origin is quantified as the first chord location at which its width is higher than 1.5*D, and corresponds to a finite distance from the element location of $\Delta x_0/c$ = 0.03 and 0.05 for Re$_{k_1}$ and Re$_{k_2}$ respectively. The Re$_{k_3}$ case introduces milder disturbances which propagate in the flow for ≃12% chord before evolving into a turbulent wedge. These results agree well with the observations of [4], identifying a finite distance between the element location and the wedge origin, which suggests that the instabilities leading to

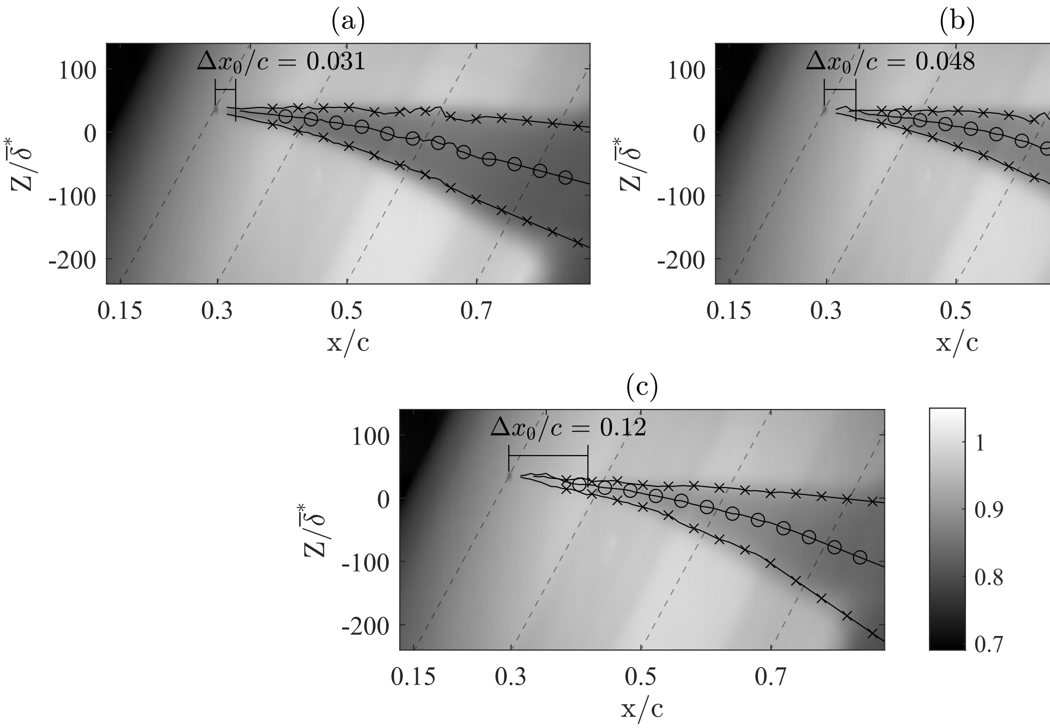

Fig. 2 IR thermography fields for forced flow cases: element located at x/c=0.15 and (a) Re$_{k_1}$=251, (b) Re$_{k_2}$=222, (c) Re$_{k_3}$=198. The flow comes from the left, linear interpolation of the wedge limits (-x); wedge middle point (-○); distance between the element and the wedge onset (Δx_0/c). Markers skipped (4 out of 5) in the chordwise direction for visualization purposes.

transition are developing in the recirculation region located aft of the element.

The extrapolation of the wedge evolution to the IR domain end is performed following a linear fit, and allows for the extraction of the wedge opening angles, laying between 8° and 12° for Re$_{k_1}$ and Re$_{k_3}$ respectively. These values are comparable with those extracted in 2D BL [e.g. 2], nonetheless the classical definition of the wedge spreading half angle is not applicable in the current investigation, since the typical symmetry of 2D BL is lost in the present set-up. More interestingly, the wedge middle point is computed along the chord in order to estimate the angle developing between the wedge and the freestream direction. This is considered to represent a measure of the overall skewness of the turbulent region development, and reaches values of 6° and 8° for decreasing Re$_k$. These angles are comparable with the angles developing between the freestream and crossflow vortices evolving in this set-up at higher Reynolds number [16–18].

B. Steady Disturbances

The analysis of the base flow development, confirms the main flow features are comparable with those of previous studies [5, 19], therefore, considering the HWA time-averaged velocity signal the developing stationary instabilities can be further analysed. The time-averaged disturbance velocity fields ($\overline{U}_d$) are reported in figure 3 for a subset of the acquired chord locations. All three Re$_k$ considered display a low momentum region developing in correspondence of the element's wake (circled in blue in figure 3), which is accompanied by two weaker low-speed streaks developing on the element sides [5, 23]. Observing their downstream evolution, the outboard (i.e. located towards higher z/$\overline{\delta}^*$ values, circled in green in figure 3) low-speed streak persists in the flow, while the wake and the inboard (i.e. located towards lower z/$\overline{\delta}^*$ values) low-speed regions are quickly decaying. Two high-speed regions are identified slightly downstream of the element location (x/c=0.17) and grow individually adjacent to the low-speed streaks. Further downstream the two high-speed streak merge, substituting the low momentum wake region [24].

To better identify the dominating stationary structures, a threshold is applied to the time-averaged disturbance fields in order to isolate the stronger high- and low- speed flow regions and their development, as showed in figure 3. The corresponding streak amplitude is estimated as their minimum (or maximum) disturbance velocity respectively. The

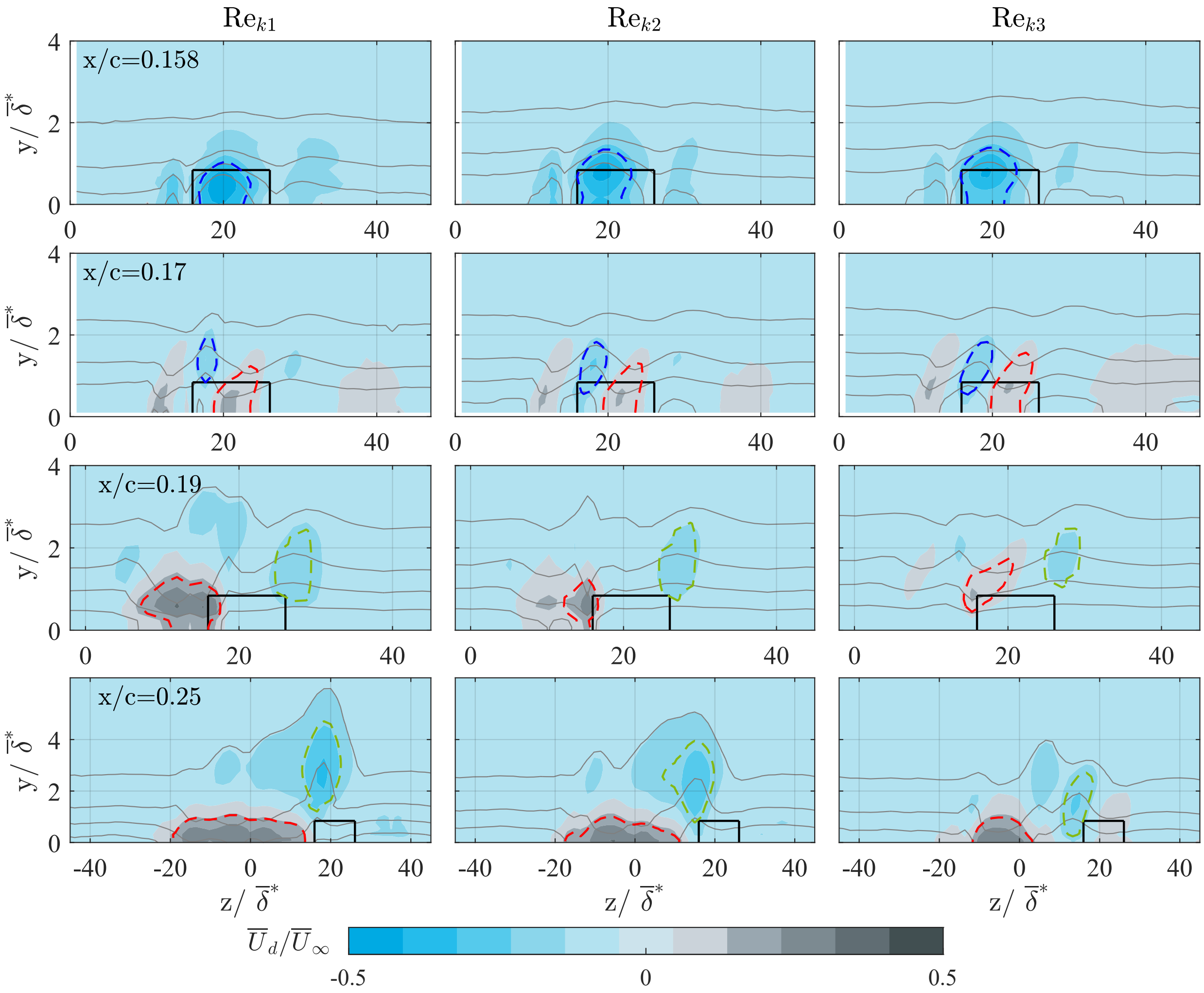

Fig. 3 HWA time-averaged disturbance velocity fields for the three Re$_k$ at different x/c locations. Low-speed region in the element's wake (blue), outboard low-speed region (green), inboard high-speed region (red). Velocity isolines plotted every 20% of $\overline{U}_\infty$ (gray lines); sketch of the element location (black rectangle).

resulting trends are collected in figure 4, confirming the previously described flow features. Namely, the low-speed region in the wake of the element is characterized by a rapid amplitude drop to null values, while the low-speed streak on the outboard side increases in magnitude. On the other hand, the high-speed structures individually grow in magnitude before merging and reaching a saturation amplitude level, which is considered indicative of the turbulence onset [7, 24].

The investigation of the stationary instabilities, proves extremely helpful towards understanding the flow topology and the chordwise evolution of the dominant flow features. However, this analysis provides only little information regarding the nature of the developing instabilities. This aspect can be further characterized investigating the unsteady velocity signal as reported hereafter.

IV. Unsteady Perturbations Characteristics

To further clarify the nature of the instabilities guiding the path towards laminar breakdown and transition to turbulence, the evolution of the unsteady disturbance fields is considered. As a starting point, the standard deviation of the HWA velocity signal (U') is analysed in order to identify the flow field regions featuring higher fluctuation, figure 5. The near-element flow fields (x/c=0.158) are characterized by a strong localized fluctuation region developing on top of the element. Investigations by [4] identified this region as the origin of the cylinder eddy shedding process,

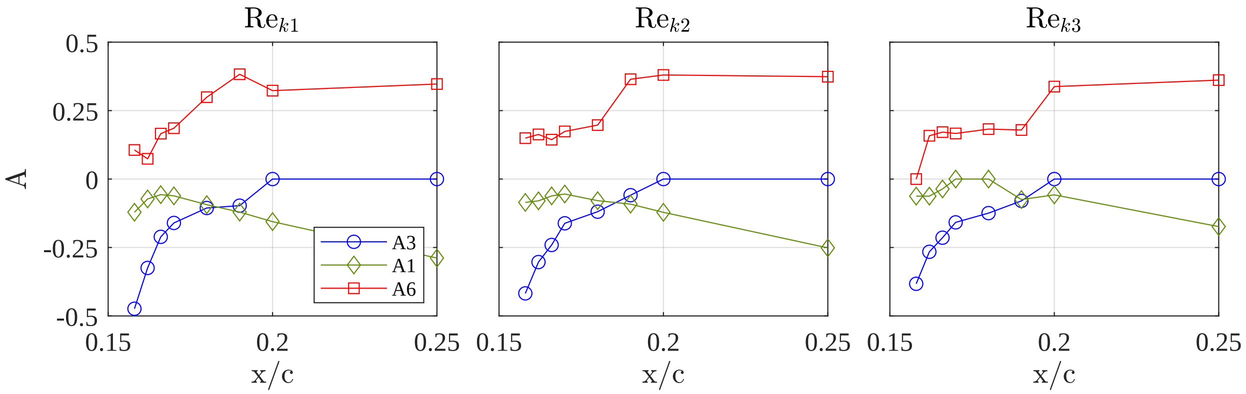

Fig. 4 Amplitude estimation of high- and low- speed streaks. Colours and symbols are identifying structures as in figure 3.

which appears to be the primary cause for the increased unsteadiness developing in the roughness element wake. A second region of weaker fluctuation amplitude is located on the element inboard side, while the rest of the flow field is characterized by almost null fluctuation amplitude values. By considering more downstream chord locations (x/c=0.162, 0.17), the oscillatory region on the element inboard side is decaying, while the unsteady region located on top of the element extends to the element flanks, possibly following the development of the horseshoe vortex legs [3, 7]. Further downstream (x/c=0.2, 0.25), the Re_{k1} and Re_{k2} cases are characterized by a broad unsteady core which rapidly spreads in the spanwise and wall-normal directions affecting a wider portion of the boundary layer flow. Comparable flow evolution characterizes also the Re_{k3} case, however the overall level of fluctuations is lower, and the unsteady core broadening occurs further downstream.

Previous investigations dedicated to isolated roughness elements [7, 13] showed that the wall-normal and spanwise velocity gradients can be insightful to identify the nature of the dominating instability. In particular, for the present case, the wall-normal mean velocity gradient is considered to have a stronger effect on the flow with respect to its spanwise counterpart, as it acts on the small length scale of the element height and on the corresponding boundary layer velocity profile modifications. Specifically, an inflection point of the base flow velocity profile, corresponds to a point of maximum or minimum of the wall-normal gradient. Hence, for each x/c flow field, at each spanwise location the wall-normal gradient profile is computed and its maximum extracted. The resulting $\frac{\partial \overline{U}}{\partial y}$ profiles extracted at a fixed spanwise location in the element's wake (i.e. $z/\overline{\delta}^*$=19.5 for x/c=0.162) are reported in figure 6 for the three considered Re_k. The standard deviation profiles and the boundary layer velocity at the same location are also included in the graphs, and confirm that the $\frac{\partial \overline{U}}{\partial y}$ maximum coincides with the point of maximum fluctuations (i.e. the U' maximum). This suggests that an inflection point, source of instabilities, should characterize the velocity profile at the same y-location. Comparable behavior is observed in the element wake region, as represented by the orange dashed line in figure 5, indicating that the developing instabilities are strongly related to the wall-normal shear layer in analogy with the observations reported by [13]. As laminar breakdown begins to affect the flow field, the observed correspondence between fluctuation amplitude and gradient maxima is lost, as already visible for x/c=0.17 in figure 5.

These considerations are further confirmed by the investigation of the time spectra of the velocity signal, extracted in correspondence to the maximum fluctuation point located on top of the element. The time-dependent signal is processed in Matlab through a Welch periodogram [25] to extract its power spectral density (PSD). The resulting spectra are reported in figure 7, and resemble the main features reported by previous studies [e.g. 4, 5, 23]. For all three Re_k considered, the spectra show a strong tonal behavior in the near-element flow. The PSD peaks correspond to dominant frequencies in the bandwidth of 1.4-1.9kHz, increasing with Re_k, and are accompanied by the development of their harmonics. However, as the laminar breakdown and the turbulence onset occur, overall higher fluctuation level is visible in the spectra, with a broader frequency distribution and no clearly identified spectral peaks. These flow mechanisms occur at approximately x/c=0.18 for Re_{k_1} and Re_{k_2}. The Re_{k_3} case retains the tonal behavior up to ≃5% chord more downstream, in agreement with previously discussed results indicating milder instabilities are developing in this case.

To effectively compare the current results with previous investigations, the Strouhal number corresponding to the identified frequency peaks is estimated. In the current analysis, the Strouhal number can be defined as $\mathrm{St}_{\overline{\delta}^*}=\mathrm{f}\times\overline{\delta}^*/|\overline{U}_\infty|$,

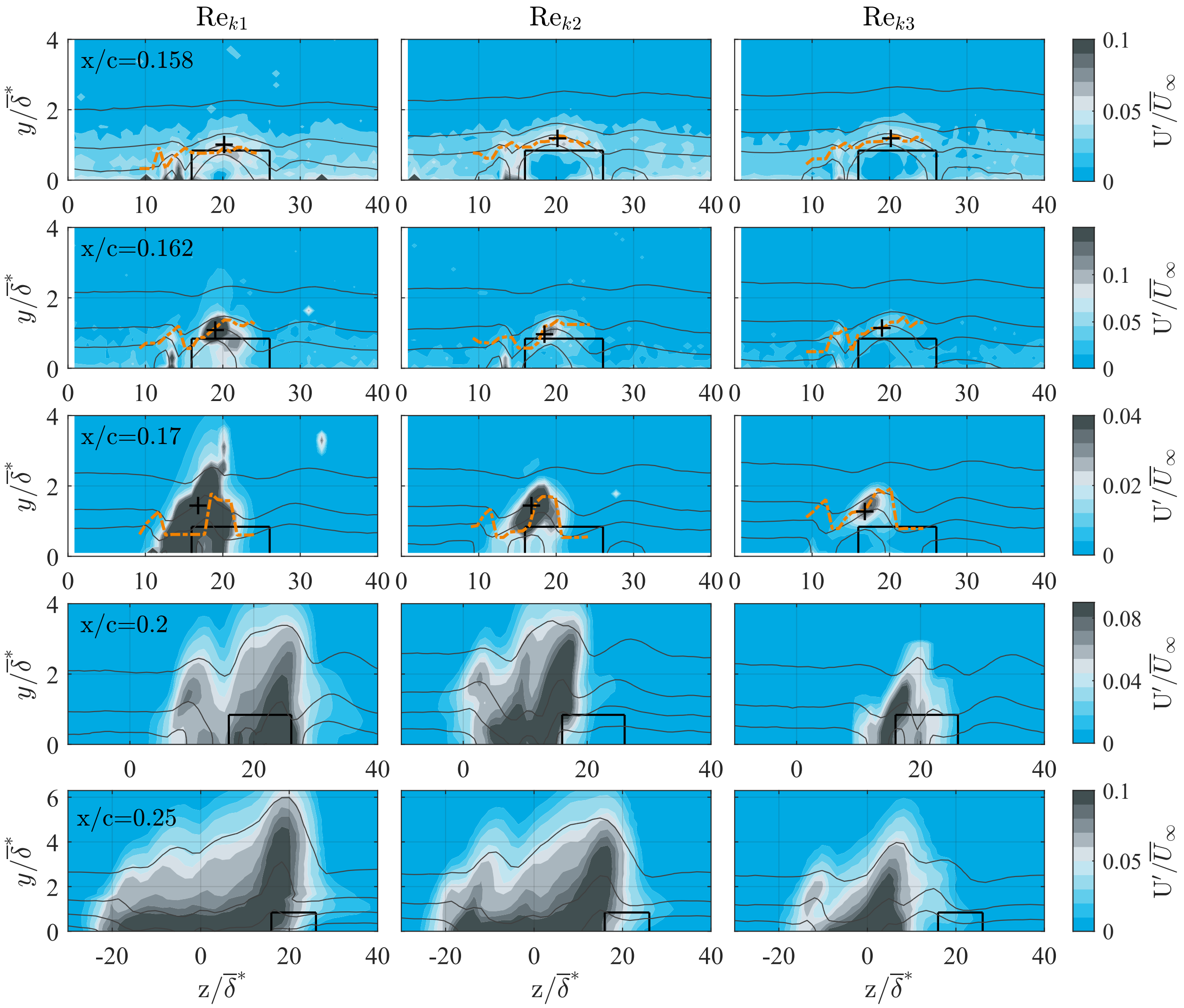

Fig. 5 HWA velocity signal standard deviation for the three Re$_k$ at different x/c location. Velocity isolines plotted every 20% of the freestream speed (full lines); wall-normal gradient maximum location (orange - - line); maximum fluctuations location on top of the element at which the spectra is extracted (+).

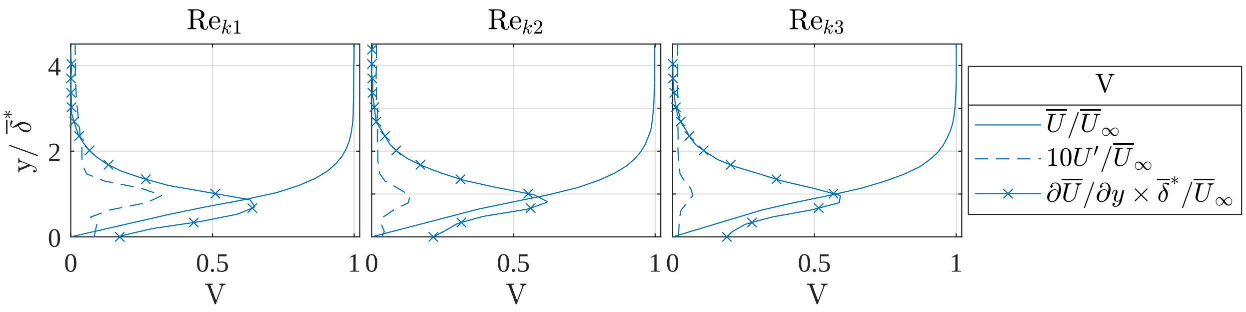

Fig. 6 Time-average velocity profile, $\frac{\partial \overline{U}}{\partial y}$ gradient profile and standard deviation profile extracted at z/$\overline{\delta}^*$=19.5, x/c=0.162 for the three considered Re$_k$.

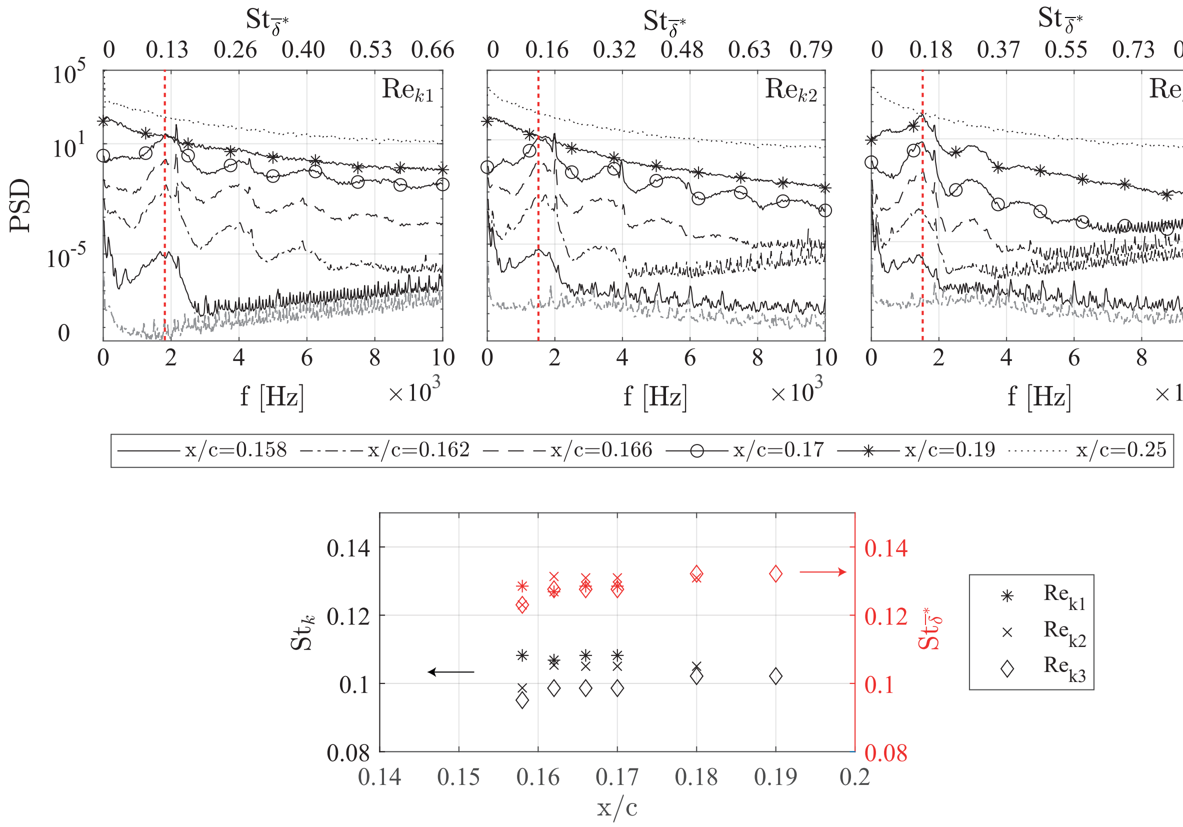

Fig. 7 Top figures: Frequency spectra extracted for different Re_k in correspondence of the maximum fluctuations region. For visualization purposes, the spectra characterizing each chord location is offset by a decade with respect to the upstream one. Freestream flow frequency spectra extracted at x/c=0.158 (gray -. line); spectral peak (red -. line). Bottom plot: St_k and $St_{\overline{\delta}^*}$ extracted for different Re_k and x/c based on the frequency peak.

or as the roughness Strouhal number $St_k = \frac{f \times k}{|\mathbf{U}_k|}$ [4, 10]. As outlined by [4], the former definition allows for the comparison of spectral modifications on a more universal scale, while the St_k depends on Re_k as it is representative for the relation between the dominant fluctuation frequencies, the element geometry and the local boundary layer development. The St number evolution is reported in the bottom graph of figure 7, and reflects the tonal behavior showed by the spectra in the near-element flow fields. Specifically, the $St_{\overline{\delta}^*}$ values lay between 0.12-0.13 for all considered cases, corresponding to the typical values associated to cylinder shedding [4]. Moreover, the St_k values mildly scale with the Re_k, and in the element vicinity are also comparable to the ones reported by [4, 5, 10], namely $St_k \simeq$0.10-0.12. This indicates that the element shedding is dominating the instability onset process. The St number values are only reported for x/c locations showing a strong tonal behavior in the extracted spectra. In fact, once laminar breakdown occurs, the tonal behavior and shedding are overcome by the increased level of fluctuations typical of a turbulent core.

In conclusion, the presented results show that the instabilities developing aft of the isolated roughness element are strongly related to the wall-normal shear layer. Moreover, the spectral analysis of the time-dependent velocity signal shows a strongly tonal behavior characterizes the near-element flow features, introducing instabilities that persist and grow in the element's wake. As evolving downstream, the turbulent flow region influences a wider portion of the boundary layer, evolving into a turbulent wedge. Based on the observed dominant frequency values and the corresponding Strouhal number values, the developing fluctuations can be related to the shedding originating on the element top, as previously observed by [4, 7].

V. Conclusions

The presented investigation is dedicated to the characterization of the instabilities and the transitional process induced by an isolated roughness element placed in a swept wing boundary layer. A single cylindrical roughness element is applied on the wing surface, and is investigated through infrared thermography and hot wire anemometry for a super-critical (Re_{k_1}) and two critical (Re_{k_2}, Re_{k_3}) scenarios.

The flow features observed in the current study are comparable to the flow topology pertaining to 2D boundary layers. In particular, the stationary flow topology can be incurred from the thermographic images as well as from the time-averaged HWA velocity signals. The near-element flow field, is characterized by the development of a low-speed flow region in the element's wake, accompanied by the development of two high-speed/low-speed streaks couples in correspondence of the wake sides. The wake low-speed region rapidly decays, substituted by the merging of the two high-speed streaks developing on the wake sides. The additional growth and saturation of the high-speed region, leads to the formation of a high-fluctuations flow region located in the element wake, which broadens as evolving downstream originating a turbulent wedge. The extraction of the high- and low-speed streaks amplitudes confirms the observed flow topology. Moreover, for the considered cases the wedge origin lays at a finite distance from the element location, which increases with a decrease of Re_k. The crossflow instabilities pertaining to the developing 3D boundary layer, are not significantly contributing to the near-element flow development. However, they play a relevant role in the downstream evolution of the turbulent flow region, which is inclined of a 6-8° angle with respect to the freestream flow direction.

Additionally, the investigation of the unsteady velocity signal indicates the presence of a high fluctuation region located on top of the element [4, 7, 18]. The analysis of the frequency spectra and wall-normal gradient evolution extracted in correspondence of the maximum fluctuation region, show a strong relation between the induced instabilities and the developing wall-normal shear layer. Moreover, a strongly tonal behavior dominates the near-element flow (upstream of the laminar breakdown), with the dominant frequency peak and its harmonics increasing with Re_k. Combining these considerations, the instabilities initiated by the roughness element appear to be of inflectional type and initiated by the shedding process occurring on the element top surface, as the St number estimation confirms.

The authors are grateful to the European Research Council for financially supporting this research through the GLOWING Starting Grant (803082).

References

[1] Gregory, N., and Walker, W., *The effect on transition of isolated surface excrescences in the boundary layer*, HM Stationery Office, 1956.

[2] Schubauer, G. B., and Klebanoff, P. S., "Contributions on the mechanics of boundary-layer transition," 1956.

[3] Baker, C., "The laminar horseshoe vortex," *Journal of fluid mechanics*, Vol. 95, No. 2, 1979, pp. 347–367.

[4] Klebanoff, P. S., Cleveland, W. G., and Tidstrom, K. D., "On the evolution of a turbulent boundary layer induced by a three-dimensional roughness element," *Journal of Fluid Mechanics*, Vol. 237, 1992, pp. 101–187. https://doi.org/10.1017/s0022112092003379.

[5] Kuester, M., and White, E., "Structure of turbulent wedges created by isolated surface roughness," *Experiment in Fluids*, Vol. 57, 2016. https://doi.org/10.1007/s00348-016-2140-x.

[6] Tani, I., "Boundary-layer transition," *Annual Review of Fluid Mechanics*, Vol. 1, No. 1, 1969, pp. 169–196.

[7] Loiseau, J., Robinet, J., Cherubini, S., and Leriche, E., "Investigation of the roughness-induced transition: global stability analyses and direct numerical simulations," *Journal of Fluid Mechanics*, Vol. 760, 2014, pp. 175–211. https://doi.org/10.1017/jfm.2014.589.

[8] Landahl, M., "A note on an algebraic instability of inviscid parallel shear flows," *Journal of Fluid Mechanics*, Vol. 98, No. 2, 1980, pp. 243–251.

[9] Chu, J., and Goldstein, D., "Investigation of turbulent wedge spreading mechanism with comparison to turbulent spots," *50th AIAA Aerospace Sciences Meeting including the New Horizons Forum and Aerospace Exposition*, 2012, p. 751.

[10] Acarlar, M., and Smith, C., "A study of hairpin vortices in a laminar boundary layer. Part 1. Hairpin vortices generated by a hemisphere protuberance," *Journal of Fluid Mechanics*, Vol. 175, 1987, pp. 1–41.

[11] Berger, A. R., McMillan, M. N., White, E. B., Suryanarayanan, S., and Goldstein, D. B., "Suppression of transition behind a discrete roughness element using a downstream element," *Tenth International Symposium on Turbulence and Shear Flow Phenomena*, Begel House Inc., 2017.

[12] Ye, Q., Schrijer, F., and Scarano, F., "Geometry Effect Of Isolated Roughness On Boundary Layer Transition Investigated By Tomographic Piv," *International Journal of Heat and Fluid Flow*, Vol. 61, 2016, pp. 31–44. https://doi.org/10.1016/j.ijheatfluidflow.2016.05.016.

[13] Ergin, F., and White, E., "Unsteady and Transitional Flows Behind Roughness Elements," *AIAA Journal*, Vol. 44, No. 11, 2006, pp. 2504–2514. https://doi.org/10.2514/1.17459.

[14] Bippes, H., "Basic experiments on transition in three-dimensional boundary layers dominated by crossflow instability," *Progress in Aerospace Sciences*, , No. 35, 1999, pp. 363–412.

[15] Saric, W., Reed, H., and White, E., "Stability and transition of three dimensional boundary layers," *Annual Review of Fluid Mechanics*, Vol. 35, No. 1, 2003, pp. 413–440. https://doi.org/10.1146/annurev.fluid.35.101101.161045.

[16] Serpieri, J., and Kotsonis, M., "Three-dimensional organisation of primary and secondary crossflow instability," *Journal of Fluid Mechanics*, Vol. 799, 2016, pp. 200–245. https://doi.org/10.1017/jfm.2016.379.

[17] Radeztsky, R., Reibert, M., and Saric, W., "Effect of Isolated Micron-Sized Roughness on Transition in Swept-Wing Flows," *AIAA Journal*, Vol. 37, No. 11, 1999, pp. 1370–1377. https://doi.org/10.2514/2.635.

[18] Brynjell-Rahkola, M., Schlatter, P., Hanifi, A., and Henningson, D., "Global Stability Analysis of a Roughness Wake in a Falkner-Skan-Cooke Boundary Layer," *Procedia IUTAM*, Vol. 14, 2015, pp. 192–200. https://doi.org/10.1016/j.piutam.2015.03.040.

[19] Kurz, H., and Kloker, M., "Mechanisms of flow tripping by discrete roughness elements in a swept-wing boundary layer," *Journal of Fluid Mechanics*, Vol. 796, 2016, pp. 158–194. https://doi.org/10.1017/jfm.2016.240.

[20] Serpieri, J., and Kotsonis, M., "Design of a swept wing wind tunnel model for study of cross-flow instability," *33rd AIAA Applied Aerodynamics Conference*, American Institute of Aeronautics and Astronautics, 2015. https://doi.org/10.2514/6.2015-2576.

[21] Serpieri, J., "Cross-Flow Instability," Ph.D. thesis, 2018. https://doi.org/10.4233/UUID:3DAC1E78-FCC3-437F-9579-048B74439F55.

[22] Munaro, F., "Mechanisms of boundary layer transition due to isolated roughness on swept wings: An experimental study," 2017.

[23] Berger, A. R., and White, E. B., "Experimental Study of the Role of High- and Low-speed Streaks in Turbulent Wedge Spreading," American Institute of Aeronautics and Astronautics, 2020. https://doi.org/10.2514/6.2020-0832.

[24] Kendall, J., "Laminar boundary layer velocity distortion by surface roughness: Effect upon stability," *AIAA paper*, Vol. 195, 1981, p. 1981.

[25] Welch, P., "The use of fast Fourier transform for the estimation of power spectra: A method based on time averaging over short, modified periodograms," *IEEE Transactions on Audio and Electroacoustics*, Vol. 15, No. 2, 1967, pp. 70–73. https://doi.org/10.1109/tau.1967.1161901.